REVIEW ARTICLE

Forced intrusion of water and aqueous solutions in microporous materials: from fundamental thermodynamics to energy storage devices†

Guillaume Fraux, [ID] [a] François-Xavier Coudert, [ID] [a] Anne Boutin [ID] [b] and Alain H. Fuchs [ID] *[a]

We review the high pressure forced intrusion studies of water in hydrophobic microporous materials such as zeolites and MOFs, a field of research that has emerged some 15 years ago and is now very active. Many of these studies are aimed at investigating the possibility of using these systems as energy storage devices. A series of all-silica zeolites (zeosil) frameworks were found suitable for reversible energy storage because of their stability with respect to hydrolysis after several water intrusion–extrusion cycles. Several microporous hydrophobic zeolite imidazolate frameworks (ZIFs) also happen to be quite stable and resistant towards hydrolysis and thus seem very promising for energy storage applications. Replacing pure water by electrolyte aqueous solutions enables to increase the stored energy by a factor close to 3, on account of the high pressure shift of the intrusion transition. In addition to the fact that aqueous solutions and microporous silica materials are environmental friendly, these systems are thus becoming increasingly interesting for the design of new energy storage devices. This review also addresses the theoretical approaches and molecular simulations performed in order to better understand the experimental behavior of nano-confined water. Molecular simulation studies showed that water condensation takes place through a genuine first-order phase transition, provided that the interconnected pores structure is 3-dimensional and sufficiently open. In an extreme confinement situations such as in ferrierite zeosil, condensation seem to take place through a continuous supercritical crossing from a diluted to a dense fluid, on account of the fact that the first-order transition line is shifted to higher pressure, and the confined water critical point is correlatively shifted to lower temperature. These molecular simulation studies suggest that the most important features of the intrusion/extrusion process can be understood in terms of equilibrium thermodynamics considerations.

1 Introduction

Porous materials such as activated carbons, carbon nanotubes, zeolites and other open framework inorganic materials have been the subject of an intense research effort in the past two or three decades, owing to their practical importance in such processes as fluid separation, ion exchange, strategic gas storage, catalysis, biosensing and controlled drug delivery. The last decade has seen the emergence of new classes of crystalline porous framework materials, based on relatively weaker chemical bonds compared to inorganic materials such

as oxides and zeolites. The most studied of these new materials today are the hybrid metal–organic frameworks (MOFs).

Most of these materials display narrow pore size, and the IUPAC recommendations[1] state that pore size under 2 nm should be called micropores, pore size between 2 and 50 nm mesopores, and pores > 50 nm macropores. Sometimes micro- and meso-pores are gathered together under the name of nanopores. Tailored nanoporous materials are still designed and synthesized at a furious pace today.

Once synthesized a new porous material must be characterized, using techniques such as X-ray diffraction, scanning electron microscopy, nuclear magnetic resonance, as well as thermogravimetric or differential scanning calorimetry. Nitrogen adsorption isotherms are measured to determine specific surface area, porous volume and pore size distribution in the general case of strongly adsorbing fluids characterized by the so called "type I" adsorption isotherms,[1] while in the opposite case of non wetting fluids a porosimetry analysis such as the mercury intrusion experiment is used.

[a] *Chimie ParisTech, PSL Research University, CNRS, Institut de Recherche de Chimie, Paris, 75005 Paris, France. E-mail: fuchs@cnrs.fr*

[b] *PASTEUR, École normale supérieure, PSL Research University, Sorbonne Universités, UPMC Univ. Paris 06, CNRS, 75005 Paris, France*

† Electronic supplementary information (ESI) available. See DOI: 10.1039/c7cs00478h

This journal is © The Royal Society of Chemistry 2017

Chem. Soc. Rev., 2017, **46**, 7421–7437 | 7421

For a long time the liquid intrusion method was used for characterizing porous materials having pore widths in the macropore range of 50 nm to 500 μm.[2] The well-established method of mercury intrusion–extrusion porosimetry relies on the Washburn equation (see Appendix) which relates the pore width to the hydraulic pressure that must be applied to the non wetting liquid to penetrate the pore. A sketch of an intrusion–extrusion porosimeter is given in Fig. 1.

Recently, in an adapted porosimetry device, water was used as a non wetting fluid to characterize hydrophobic nanoporous materials such as silica gels[3] and siliceous zeolites,[4,5] or micelle-templated silica.[6] A new field of research emerged from these studies,[4–9] which is still active today. More recently, forced wetting of electrolyte solutions was studied, disclosing very interesting giant osmotic pressure effects.[10,11]

In the present article we first review these forced intrusion studies of water in microporous materials such as zeolites and MOFs. Many of these studies were aimed at investigating the possibility of using these systems as energy storage devices. Some efforts have been made recently to investigate the possible design of a proper damper or shock absorber for practical usage, and these studies will be reviewed here.

This review also addresses the theoretical approaches and molecular simulations of confined water performed in order to better understand the experimental behavior of water confined in nanopores. The behavior of water confined to spaces of nanoscopic dimensions is an important issue in many areas of science and technology.[12,13] The aim is to understand the changes in water properties due to interactions with a hydrophobic substrate, as well as the modifications in its properties

Guillaume Fraux is a PhD student at Chimie ParisTech/PSL Research University. He did his undergraduate studies in the Chemistry department at École normale supérieure in Paris. He is now working on the development and implementation of molecular simulation methods for the study of intrusion, adsorption, and deformation in soft porous crystals. Besides being a PhD student with many simulations running, he is also programmer

Guillaume Fraux

for many projects, and the principal author of the chemfiles library (http://chemfiles.org/), providing read and write capabilities for chemistry file formats to other programmers. Find him online at http://guillaume.fraux.fr.

FX is a CNRS researcher at Chimie ParisTech/PSL Research University, in Paris (France). His main research interests lie in the computational study of materials and interfaces, with specific focus on developing molecular simulations methods and statistical thermodynamics models to describe the adsorption of molecular fluids in zeolites, metal−organic frameworks, and other nanoporous materials. In particular, he loves flexibility, defects, disorder, and all entropy-

François-Xavier Coudert

related things. He doesn't like: writing about himself in third person. See http://coudert.name/ for further details, or follow him on www.twitter.com/fxcoudert.

Anne Boutin is a research director at CNRS and professor at École Normale Supérieure (ENS), part of PSL Research University (Paris, France). She is a specialist in molecular thermodynamics. She develops and uses simulation tools as well as theoretical approaches to study various phenomena affecting the structure, dynamics, thermodynamics and reactivity of condensed phases, most often of confined molecular fluids. She obtained her PhD in physical

Anne Boutin

chemistry from the University of Paris-Sud in 1992. She joined the CNRS in 1994. After a first part of her career in Orsay, she joined the ENS in 2009 and heads the Department of Chemistry since 2014.

Prof. Alain Fuchs studied chemistry at EPFL, Lausanne and received his PhD in physical chemistry at the University Paris-Sud, Orsay France in 1983. After a postdoctoral stay at the University of Edinburgh with Stuart Pawley, he was appointed as a research fellow at the French CNRS. He became Professor of chemistry at Université Paris-Sud in 1996 and director of ENSCP, a graduate school of chemistry and chemical engineer, in 2006. He was

Alain H. Fuchs

appointed in 2010 as the President of CNRS, and elected in 2017 as President of PSL Research University. He is a fellow of the Royal Society of Chemistry and a member of the Academia Europea.
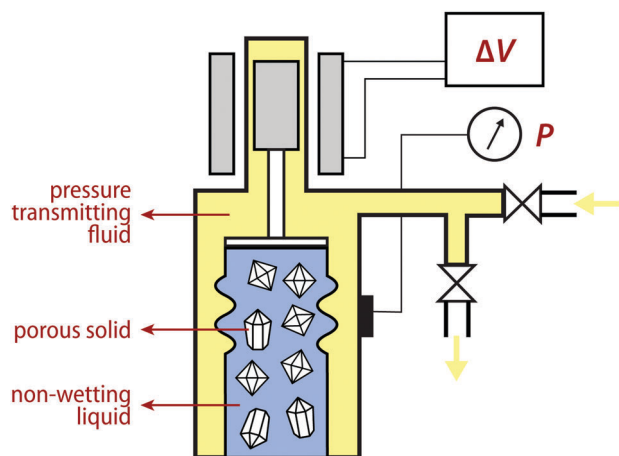
Fig. 1 Sketch of an intrusion–extrusion porosimeter. A sample of porous solid powder is placed in a non-wetting liquid (in blue) and pumps control the pressure of a pressure-transmitting fluid (in yellow). A manometer records the pressure P during the experiment, and a transducer records changes in volume of the system. The total change in the volume is then corrected for the compressibility of the non-wetting liquid and pressure-transmitting fluid, in order to obtain the volume of non-wetting liquid intruded into the porous solid.

due to the geometric confinement effect—such as changes in the structure,[14] dynamics,[15] or phase diagram.[16] This is relevant to such problems as selective adsorption using activated carbons or all-silica zeolites[17,18] (waste water treatment for instance). Similar questions arise when considering the issue of confined water in biological channels[19,20] and protein cavities.[21,22] We shall use for the rest of this article the term hydrophobic solid to depict a porous solid, the internal surface of which is hydrophobic, meaning that the potential energy interaction between the water molecules and the confining solid wall is much weaker than the water molecules' mutual interaction. This is typically the case when the adsorption enthalpy, ΔH_{ads}, or the isosteric heat of adsorption at low uptake, q_{st}^0, is small compared to the water enthalpy of vaporization, ΔH_{vap} (which is 41 kJ mol^{-1} at 373 K).

We also review the recent experimental advances in which the pressure transmitting fluid does not enter the pore space of the material but instead induces a structural transformation. Porosimetry devices are also being used in some of these works in order to apply a hydrostatic pressure to the powdered nanoporous crystalline samples. The first known example of such an experiment is the study of the pressure induced structural transition in MIL-53(Cr) metal–organic framework using a mercury porosimeter.[23] Such systems can also be thought of as energy storage devices. In recent years several studies have investigated this possibility.[24–27]

These latter studies display some interesting links with the pressure-induced hydration (PIH) and pressure-induced phase transformations (PIPTs) investigations, using Diamond Anvil Cells (DAC), which we will discuss briefly. Structural transitions or amorphization in MOFs and ZIFs materials (zeolitic imidazolate frameworks) are also currently studied.[28–32] DAC and porosimeters are complementary to each other.

Porosimeter experiments provide thermophysical information such as the intrusion/transition pressure as well as the transition heat and mechanical work involved in the transformations.[27] DAC experiments on the other hand allow structural and spectrometry analysis such as X-ray diffraction (XRD) or Raman scattering. Some recent studies use both techniques[24] and it would be desirable to device an instrument that would allow to obtain all the necessary information at the same time.

Finally, the basics of thermodynamics of confined fluids are summarized in the Appendix.

2 Forced intrusion of water in microporous solids and energy-storage devices

2.1 The silicalite-1 (MFI)–water system

The general idea of storing energy by forced intrusion of a non wetting fluids in porous media was first explored by Eroshenko some years ago.[3,33] In 2001, Eroshenko et al.[4] published a seminal paper in which they reported a stepwise intrusion–extrusion of water in two different hydrophobic zeolites (also called zeosil), namely zeolite β and silicalite-1 at pressures of $\simeq 60$ and 80 MPa respectively, i.e. notably above the water saturation pressure of 3500 Pa at room temperature. In addition, they showed that the water intrusion pressure was shifted to higher pressure ($\simeq 100$ MPa) when using a sample of silicalite-1 synthesized through the fluoride (F$^-$) route. We will get back to this point later on. The structures of both zeolites are presented in Fig. 2.

The reported results are reproduced in Fig. 3. For comparison sake, an experiment was performed using a standard ZSM-5 hydrophilic zeolite which does not display the intrusion–extrusion phenomenon. A small hysteresis phenomenon was observed in the case of silicalite-1 (MFI-type structure), while zeolite β (*BEA-type structure, whose name is marked with an asterisk because it is a partially disordered framework) behaved very differently. Upon pressure release, water appeared to be stuck into the zeolite framework, something that is reminiscent of some mercury intrusion–extrusion experiments performed in macroporous solids.[2] The authors concluded from these results that it was possible to use these heterogeneous systems to "accumulate, restore and dissipate mechanical energy", thus opening new routes in the field of energetics. In terms of energy
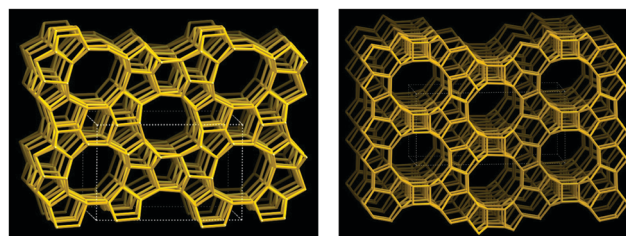

Fig. 2 Structure of the silicalite-1, or MFI zeolitic network (left) and the zeolite β, or *BEA network (right). Each vertex of the network is a silicon atom, and each edge corresponds to a Si–O–Si bridge.
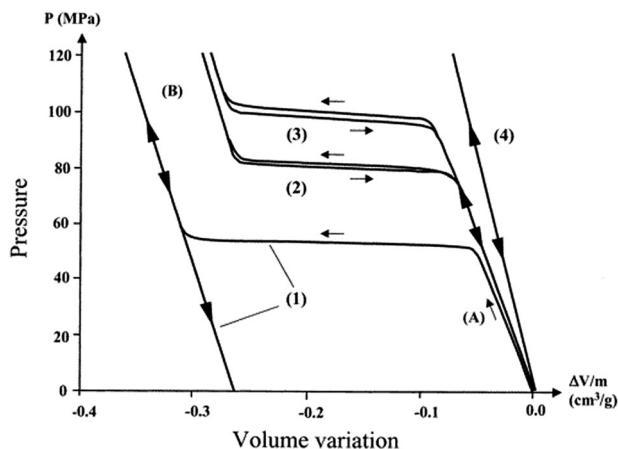
Fig. 3 Pressure–volume isotherm of the various "water-hydrophobic zeolite" systems. (1) "water–zeolite β" system. (2) "water–silicalite-1 (OH⁻)" system. (3) "water–silicalite-1 (F⁻)" system. (4) "water–Na-ZSM-5" system. (A) Step before intrusion. (B) Step after intrusion. In these experimental curves, the pressure is along the y axis and the volume variation (along the x axis) is negative, indicating the compression of the total system. The data are not corrected to account for compressibility of the water. Reproduced with permission from ref. 4. Copyright 2001 American Chemical Society.

Fig. 4 ^{1}H MAS NMR spectrum of (top) calcined silicalite-1 (F⁻); (middle) calcined silicalite-1 (OH⁻); (bottom) calcined commercial sample. Reproduced with permission from ref. 4. Copyright 2007 American Chemical Society.

storage devices, a system displaying an intrusion–extrusion cycle without hysteresis can simply be termed as a "spring". A system with hysteresis is a "shock absorber" and an incomplete cycle in which water is retained in the porous framework upon pressure release can be called a "bumper".

This seminal work raised several interesting and important questions. First of all, from a fundamental thermodynamics point of view, the occurrence of a sudden, stepwise, first-order like transition such as the observed intrusion–extrusion cycle of Fig. 3 was not expected in such solids with extremely narrow pores. It has been accepted for long in the adsorption community, that there was no capillary condensation in micropores,[1] and that the term capillary (or pore) condensation should not be used to describe micropore filling because "it does not involve a vapor–liquid phase transition".[34] In the present case, water intrusion in zeolite cannot be assigned to capillary condensation, since it takes place above the water saturation vapor pressure, but more likely to a capillary evaporation phenomenon.[35] Nevertheless, such a first-order transition remains unexpected in such narrow pores, for the same reasons given above. The issue raised by the observed stepwise transition shown in Fig. 3 obviously needed a thorough theoretical analysis. This is developed in Section 2.3 below.

From the experimental point of view, there was a need for an in-depth analysis of the water–silicalite-1 system and it was also important to investigate other water–hydrophobic zeolites systems in order to ascertain how general the sudden intrusion–extrusion phenomenon was, and how it changed from one zeolite to another. The group of Patarin and coworkers in Mulhouse (France) is central to these studies since they have devised very efficient tools devoted to the synthesis and characterization of hydrophobic materials.
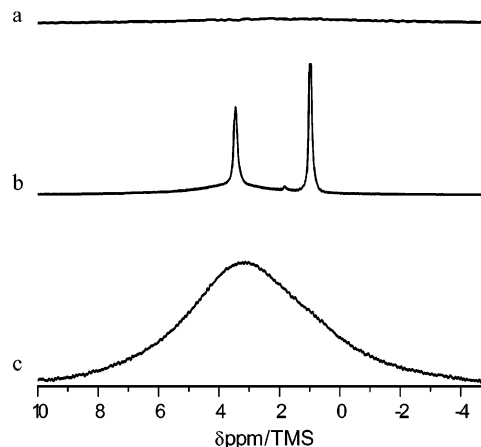
Silicalite-1 (MFI) zeolite can be synthesized with very few chemical defects (mostly silanol groups). These silanol defects are formed by hydrolysis of the Si–O bonds inside the structure of the zeolite, following the reaction $Si–(O–Si)_4 + 2H_2O = 4SiOH + SiO_2$. Silanol groups forming the crystal surface and terminating the crystal are different from defects in the bulk of the crystal. The low number of silanol defects was demonstrated by the investigation of three types of samples: a commercial silicalite-1 sample, a sample prepared in alkaline medium (silicalite-1 (OH⁻))[36] and a third sample prepared in fluoride medium (silicalite-1 (F⁻)).[37] Trzpit et al.[38] performed NMR experiments on these three samples and confirmed that the zeolite obtained through the fluoride route contained the lowest proportion of hydrophilic silanol defects, as shown in Fig. 4. The synthesis procedures and characterizations are fully described in ref. 38.

The corresponding liquid phase water intrusion–extrusion experiments are shown in Fig. 5. The water–silicalite (F⁻) system displays a reversible and rather steep intrusion–extrusion transition at ≃100 MPa, confirming the previous investigations,[3] except that no hysteresis was observed in this sample. In the more defective, and less hydrophobic samples (OH⁻ and commercial) the condensation transition is gradually shifted to lower pressures and is accompanied by a pronounced rounding.

A set of Monte Carlo simulations enabled to shed some light into this phenomenon at the molecular level.[38] In these simulations, an all-silica silicalite-1 model with no defect displayed a sudden first-order like condensation transition, as it will be detailed below in the section devoted to the theoretical approaches. The introduction of a growing number of model silanol defects in the simulations lead to a shift and rounding of the transition, in much the same way as in the experiments.[38,39]

The picture that emerged from this intensive study of silicalite-1 (MFI) is that of a first-order intrusion–extrusion transition, which is often shifted and rounded due to the unavoidable existence of a various amount of hydrophilic defects in the samples. The fact that a water intrusion
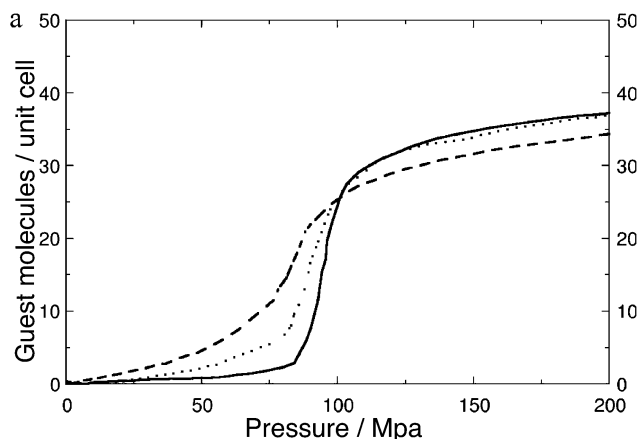
7424 | Chem. Soc. Rev., 2017, 46, 7421–7437

This journal is © The Royal Society of Chemistry 2017

Fig. 5 Experimental water intrusion–extrusion in silicalite-1 (MFI) samples. Full line: silicalite-1 (F⁻); dotted line: silicalite-1 (OH⁻); dashed line: commercial sample. Compared to Fig. 3, this representation of the intrusion–extrusion curves has a different choice of axes: pressure is along the x axis, while intruded quantity of water (guest uptake, which is proportional to the intruded volume) is indicated along the y axis. For this system, the value of 50 molecules per unit cell corresponds to 0.156 mL g^{-1} of intruded liquid. Reproduced with permission from ref. 4. Copyright 2007 American Chemical Society.

transition can be shifted by up to some 50 MPa in defects containing materials is an important point for the discussion to follow.

2.2 Other zeosil–water systems

An important number of other all-silica zeolites (zeosil) was investigated by the Patarin group over the years, from 2001 until very recently.[40–50] They are gathered in Table 1, together with the main intrusion–extrusion properties. As already mentioned the energy storage behavior can either be depicted as a "spring" (S) when the intrusion–extrusion cycle is fully reversible, a "shock absorber" (SA) when the cycle displays an
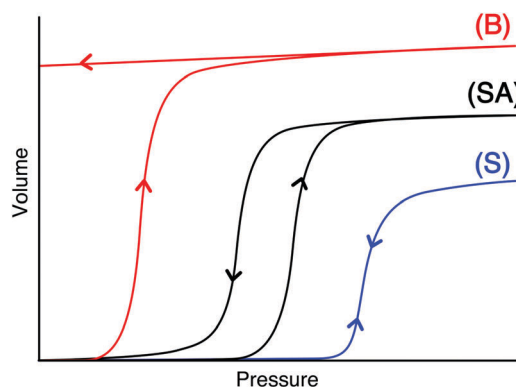

Fig. 6 Schematic representation of the 3 different types of energy storage behavior: Spring (S), Shock Absorber (SA) and Bumper (B). The intruded volume of liquid is represented along the y axis (as positive values), as a function of external pressure.

hysteresis, or a "bumper" (B), when the cycle is incomplete and some water is retained in the porous framework upon pressure release. This is shown schematically in Fig. 6.

In several cases, the zeosil–water system displays a narrow hysteresis (*i.e.* a few MPa at most). It behaves then almost like a spring and is termed S$_{(SA)}$ in Table 1. In the case of chabazite (CHA) the intrusion–extrusion behavior is close to a spring even though there is a small (but noticeable) quantity of water ($\simeq 6\%$) retained in the framework upon pressure release after the first cycle. It is thus termed S$_{(B)}$ in Table 1.

The properties of the different zeosil–water systems, reported in Table 1, may be first rationalized in terms of the stability of the frameworks upon water intrusion with respect to hydrolysis. Careful powder XRD, ^{1}H/^{29}Si solid state NMR and thermogravimetric analysis[4,18,38,41,42,44,47] have shown that the zeosil gathered in the upper part of Table 1 display a good resistance to hydrolysis, at least after a few intrusion–extrusion

Table 1 Energy storage behavior (see text) and values of the intrusion pressure, extrusion pressure and stored energy for the different zeosil–water systems reported in the literature. Each structure type is represented graphically in the ESI. The largest cavity radius is taken from ref. 51. The spreading of the intrusion transition is also reported for each system. Its value is estimated from the published intrusion–extrusion figures. These are approximate values, and are here to show that some zeosil–water systems, namely FER, MTW and TON, exhibit a very large spreading of the intrusion transition. The upper part of the table corresponds to zeosil frameworks that are resistant to hydrolysis. In the lower panel, ISV, RRO, STT and to a certain extend CHA are unstable upon water intrusion.[40,43,45,49] *BEA, BEC and LTA display a clear bumper behavior

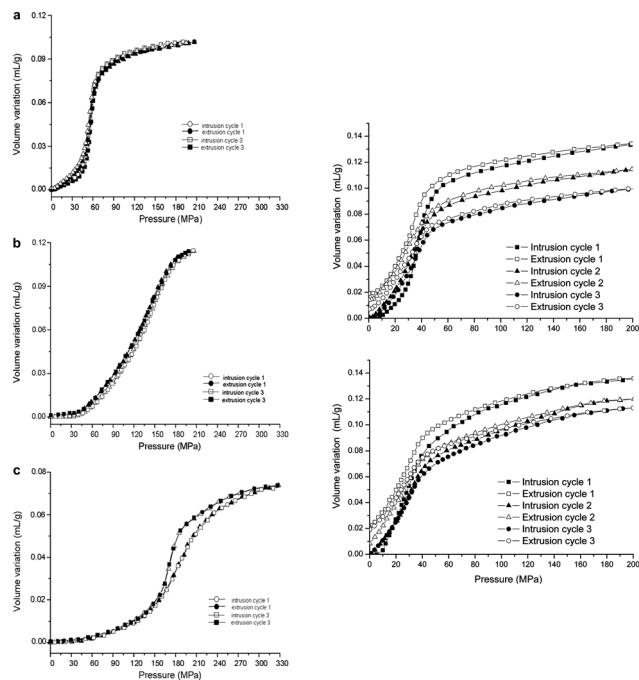| Structure type	Ref.	Energy storage behaviour	Intrusion pressure (MPa)	Extrusion pressure (MPa)	Stored energy (J g^{-1})	Largest cavity radius (Å)	Intrusion spreading (MPa)
AFI	42	S	57	57	5.8	4.15	$\simeq 0$
DDR	47	S$_{(SA)}$	60	51	6.7	3.83	20
MEL	44	S$_{(SA)}$	63	58	6.5	3.86	70
MFI	4, 7 and 38	S$_{(SA)}$	96	91	10.6	3.18	$\simeq 0$
MTW	42	S	130	130	15.0	3.04	140
FER	41	S$_{(SA)}$	147	142	15.0	3.15	120
TON	42 and 52	SA	186	172	14.0	2.85	200
CHA	40	S$_{(B)}$	37	31	5.5	3.68	20
ISV	45	SA	—	—	—	3.50	—
RRO	49	SA	—	—	—	2.23	—
STT	43	B	—	—	—	3.52	—
*BEA	4 and 50	B	53	—	8.3	3.34	$\simeq 0$
BEC	46	B	41	—	3.3	3.48	30
LTA	48	B	25	—	3.4	5.53	30

Fig. 7 Successive experimental intrusion–extrusion cycles of AFI, MTW and TON (left panel) and STT (F) and STT (OH) (right panel) zeosil–water systems. Left panel: Reproduced from ref. 42 with permission from Elsevier. Right panel: Reproduced with permission from ref. 43. Copyright 2012 American Chemical Society.

cycles. This means that the framework structures, fully characterized before and after water intrusion, are unaltered and consequently the successive cycles of intrusion–extrusion isotherms are superimposed to each other, as shown in Fig. 7 in the case of the AFI, MTW and TON-type zeosils.

The lower panel of Table 1 corresponds to zeosil frameworks that are clearly affected by water intrusion. This is revealed by the formation of silanol defects in the internal surface of the zeosil framework, due to the breaking of siloxane bridges, as evidenced by NMR spectroscopy. As a consequence, the successive intrusion–extrusion cycles differ from each other, as shown in Fig. 7, in the case of SSZ-type zeosils (synthesized in the fluorine or in the hydroxyl routes respectively). ITQ zeosil was also found to behave like a bumper on account of the formation of silanol defects upon water intrusion.[52]

Overall, the group of J. Patarin has identified a certain number of zeosil frameworks, namely AFI, DDR, MEL, MFI, MTW, FER and TON, which were found suitable for reversible energy storage because of their stability with respect to hydrolysis after several water intrusion–extrusion cycles. This aspect will be further discussed below in the section devoted to energy storage devices.

2.3 Insights from theory and molecular simulation

Grand Canonical Monte Carlo (GCMC) simulations were first performed by Desbiens et al.[53,77] who were able to reproduce the water intrusion–extrusion step-wise transition in silicalite-1 (MFI). This phenomenon was tentatively interpreted in terms of

an equilibrium first-order vapor–liquid condensation, following Porcheron et al.,[35] who pointed out the similarity between capillary condensation of a wetting fluid and forced intrusion of a non wetting fluid. However, no firm evidence was provided for the actual thermodynamic status of this transition. In addition, water intrusion takes place experimentally in a much more continuous way in MTW, FER and TON than in MFI and AFI for instance (see Fig. 7). In Table 1 we have reported the spreading of the intrusion transition for the different experimentally studied zeosils. The intrusion transition is steep for AFI and MFI and weakly rounded for DDR. This can tentatively be accounted for by the existence of a small proportion of hydrophilic silanol-like defects, as seen above in Fig. 5. The least hydrophobic MFI sample for instance exhibits an intrusion spreading of some 70 MPa. The case of MEL might then be included in the same category. In contrast, MTW, FER and TON display huge intrusion spreading of 120 to 200 MPa which seemed difficult to attribute to a defect-induced rounding of the transition.

Cailliez et al.[41] investigated in some details the intrusion–extrusion transition in silicalite-1 (MFI, channel's diameter of 5.4 Å) and ferrierite (FER, ellipsoidal channels of dimensions 4.1 × 5.4 Å). They first computed the volume–pressure isotherm using GCMC simulations. The results are shown in Fig. 8.

The pressure values at which the simulated condensation processes take place in these two zeosils are underestimated by 30 to 50%. However, this deviation corresponds to a 2–4% difference in chemical potential only. This is due to the fact that $(\partial\mu/\partial P)_T$ is quite small in the liquid phase.[5,38] Given the crudeness of the model (e.g. rigid framework, see ref. 41 for the simulation models and methods), these results were considered satisfactory. The intrusion pressure at room temperature was shown to be extremely sensitive for instance to small
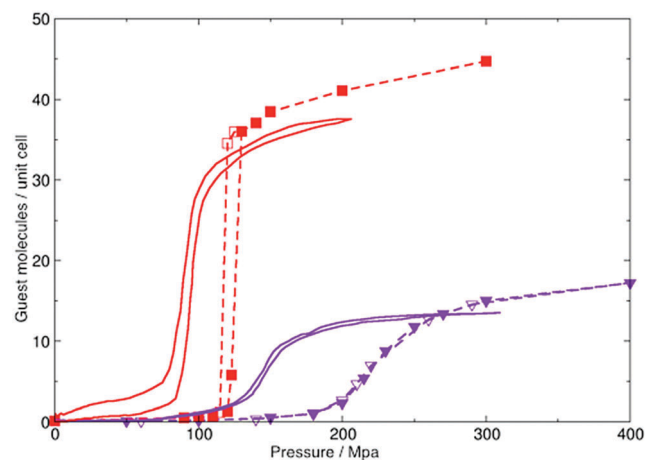

Fig. 8 Water intrusion/extrusion isotherms in silicalite-1 (MFI, red and squares) and ferrierite (FER, purple and triangles). Experimental data are shown in plain lines, symbols represent GCMC simulations (filled symbols: intrusion, open symbols: extrusion). Reproduced from ref. 41 with permission from the PCCP Owner Societies. For the silicalite-1/water system, 50 molecules per unit cell correspond to 0.156 mL g^{-1}; and for the ferrierite/water system, 20 molecules per unit cell is 0.166 mL g^{-1}.
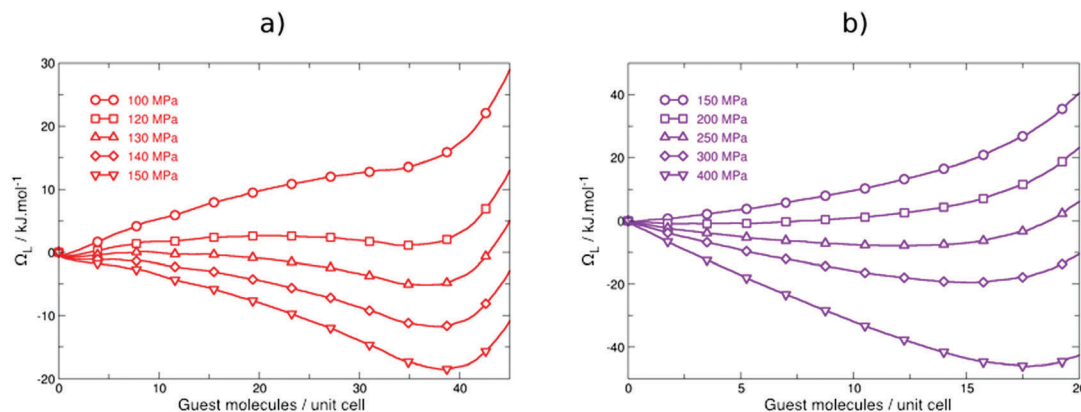
7426 | Chem. Soc. Rev., 2017, 46, 7421–7437

This journal is © The Royal Society of Chemistry 2017

Fig. 9 Computed free energy Ω_L of the water–zeolite system for various pressure at 300 K, as a function of the amount of intruded water; (a) MFI, (b) FER. Reproduced from ref. 41 with permission from the PCCP Owner Societies.

changes in the framework atomic coordinates.[54] The main finding reported in Fig. 8 is that the GCMC simulations were able to qualitatively reproduce the large spreading of the water intrusion process in ferrierite (FER) while at the same time the intrusion phenomenon in silicalite-1 (MFI) was much steeper.

Cailliez *et al.*[41] also examined in more details the nature of the condensation transition in both cases, in order to better understand the underlying physics that causes intrusion to be either an abrupt or a much more continuous process, depending on the extent of the fluid confinement. They computed the Landau free energy Ω_L as a function of the number of intruded water molecules for various pressure, at 300 K, using the Wang–Landau method based on the computation of the Density of States (DOS) on-the-fly, using Monte Carlo simulations with non-Boltzmann sampling.

The Landau free energy Ω_L is reported in Fig. 9 as a function of the number of intruded water molecules for various pressures, at 300 K. The water–MFI system (Fig. 9a), is characterized by the existence of a double potential well. Below 120 MPa, the most stable state corresponds to the empty zeolite, and the filled state is metastable. Above 120 MPa, the filled state has become the most stable one. The existence of two stable states is characteristic of a first-order transition between gas-like and liquid-like phases. The conversion between those two states is possible on a wide range of pressure as seen in Fig. 9a, but the system has to overcome a macroscopic energy barrier. Monte Carlo simulations proceed *via* microscopic moves. In a finite time Monte Carlo run, the most stable state may not be reached, and this is why a small hysteresis loop is observed.

In contrast, the water–FER system (Fig. 9b) displays only one stable potential well. At 150 MPa the stable state is the empty zeolite. As pressure increases, the single stable state progressively moves along the N coordinate until the porous framework is completely filled ($\simeq 400$ MPa). This feature is reminiscent of a continuous phase transition, although there are other possible explanations. For instance the increased fluid confinement may lead to a pseudo 2D, or even 1D behavior, for which it is known that the conventional views of the bulk phase transitions are no more valid.

Further insights were provided by the same authors with a study of the effect of temperature on the intrusion transition. A change in the shape of the isotherm as temperature is increased from 300 to 400 K was observed in the case of MFI. From first-order, the transition becomes continuous-like. Conversely the continuous transition in FER at 300 K (a single potential well), turns into a first-order transition (double well behavior) as temperature is decreased to 200 K.[41]

The above results were interpreted in terms of the existence of a genuine first-order vapor–liquid transition line terminated by a critical point. A schematic phase diagram of confined water in zeolites was proposed and is shown in Fig. 10. In this tentative diagram, the vapor–liquid transition is schematically described and the solid–liquid and solid–gas transitions are not considered in any details. This diagram is based on two simple assumptions related to fluid confinement in a hydrophobic solid: a shift of the vapor–liquid transition to higher pressure as confinement increases together with a shift of the critical point to lower temperature.[55] This provides a plausible qualitative explanation of the fact that, at 300 K, the vapor–liquid transition is first-order like in MFI, while it turns into a smooth, supercritical, crossing from a diluted to a dense fluid in the case of FER.
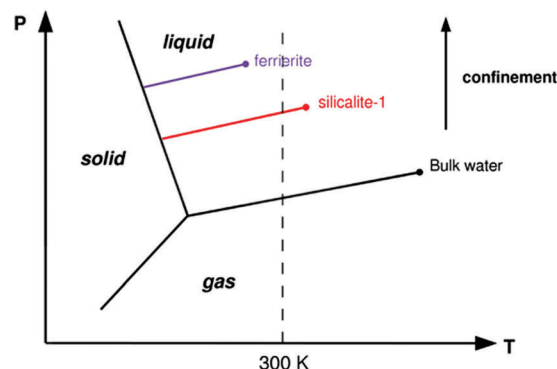

Fig. 10 Schematic phase diagram of confined water in MFI and FER zeosils. Reproduced from ref. 41 with permission from the PCCP Owner Societies.

This journal is © The Royal Society of Chemistry 2017

Chem. Soc. Rev., 2017, **46**, 7421–7437 | **7427**

It might appear surprising that a bulk fluid phase diagram can be extended in such a way, down to the nanoscale range. Indeed, it is common wisdom, in the adsorption community, that the usual bulk phase transitions do not exist anymore in micropores,[1,34] and especially so in zeolites. Experimentalists, in the adsorption community, are usually restricting the use of capillary condensation to describe the filling of mesopores and macropores (*i.e.* in pores of widths >2 nm). Adsorption in microporous solids (pore widths <2 nm) are usually characterized by reversible type-I isotherms. This view is valid for the adsorption of fluids that have a strong affinity with the adsorbent walls (it is typically the case in aluminosilicate zeolites). For large enough pores, surface wetting (or layering) occurs at low pressure, in undersaturated vapor. It is followed at higher vapor pressure by the fluid condensation in the pore interior. In their influential textbook on adsorption, Rouquerol, Rouquerol and Sing (page 444 in the 1999 Edition),[1] describe capillary condensation as a ''secondary process, which is always preceded by adsorption on the pore walls''. What was learn from the physics of phase transitions is that only for large pores can the surface and bulk effects be separated. An increasing mixture of surface and bulk transitions is known to take place as the pore narrows.[55,56] This explains why capillary condensation cannot be distinguished anymore from surface wetting in strongly adsorbing microporous materials. The situation in which the fluid does not fully wet the pore surface is different. In this case, a first-order like condensation of the fluid can be observed, provided that the interconnected pore structure is 3-dimensional and sufficiently open. In their study of MFI Desbiens *et al.*[7] observed that the transition occurred everywhere in the porous solid, at the same pressure. Even though each channel portion of the presently studied zeolites forms a pseudo 1D confined system in which a first-order transition is theoretically forbidden, the interconnected nature of the porous structure and the correlation between adjacent pores[57] ensures a 3D-like behavior of confined water. The occurrence of such a first order-like transition has actually been predicted by Bichara and Pellenq[58,59] in the case of selenium adsorption in silicalite-1 zeolite. A simulation of water confined to narrow carbon nanotubes has also revealed discontinuous as well as continuous solid–liquid phase changes.[60] More recently, Braun *et al.*[61] demonstrated, using NMR relaxometry and molecular dynamics, that a true liquid–vapor coexistence existed in fluid benzene confined in IRMOF-1 metal–organic framework. The liquid and vapor phases were shown to extend over many unit cells thanks to the open 3D framework, as shown in Fig. 11. These results enabled to explain the adsorption data of cyclohexane and CO_2 in IRMOF materials,[62,63] and are consistent with the GCMC study of de Toni *et al.*[64]

The main conclusion of these molecular simulation studies is that water condensation takes place through a genuine first-order phase transition, provided that the interconnected pores structure is 3-dimensional and sufficiently open. In extreme confinement situations (such as in FER zeosil), condensation may take place through a continuous supercritical crossing from a diluted to a dense fluid, on account of the fact that the
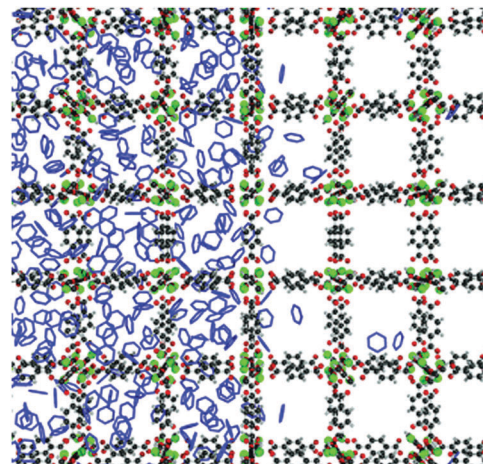

Fig. 11 A snapshot of the molecular dynamics simulation of benzene in IRMOF-1 metal–organic framework. A vapor–liquid coexistence takes place, the vapor and liquid phases extending over many unit cells. Reproduced from ref. 61.

first-order transition line is shifted to higher pressure, and the confined water critical point is shifted to lower temperature. We also note in passing that the confined water phase, as observed in the molecular simulation studies, is depleted with respect to bulk water (a density of $\simeq 0.6$ in the MFI–water system).[7,53]

In the intrusion experiments, a rather high hydraulic pressure must be applied until the sudden fluid penetration takes place. This has lead to several interpretations of this phenomenon in terms of irreversibilities.[4,5,65] Only recently has this process been examined in the light of equilibrium statistical thermodynamics.[66] The similarity between capillary condensation of a wetting fluid and forced intrusion of a non wetting fluid was, for a long time, overlooked.[35] What these molecular simulation studies suggest is that the most important features of the intrusion/extrusion process can be understood in terms of equilibrium thermodynamics considerations. Water intrusion is a first order vapor–liquid transition that takes place above the saturation vapor pressure because the water–solid interface in non-wetting. The accompanied heat effect is either endothermic or exothermic,[64,67–69] depending on the pore size of the hydrophobic materials, and Cailliez *et al.*[41] showed that it could be accounted for by considering the changes in internal energy of water inside as well as outside the porous solid.

Finally, we address the issue of understanding the change in intrusion pressure with the framework properties. Several years ago, Lefevre *et al.*[6] investigated the intrusion–extrusion transition of water in hydrophobic mesoporous materials characterized by independent cylindrical pores (the so-called MCM-41 material). They showed that the intrusion was well described using a macroscopic capillary model, the intrusion pressure increasing linearly with the inverse of the pore radius, as predicted by the Washburn equation (see eqn (4) in Appendix). These results are shown in Fig. 12. It was rather surprising at that stage to observe that the classical Washburn equation was still valid down to pore radius ranging from 13 to 54 Å. In the case of microporous zeosil materials, Tzanis *et al.*[44] have found
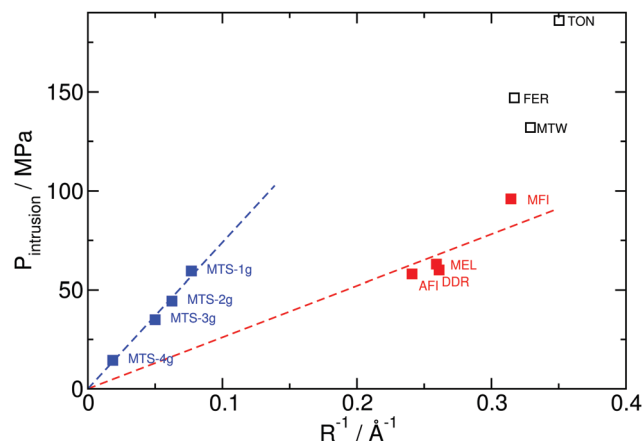
Fig. 12 Water intrusion pressure as a function of the inverse radius R. The blue dots correspond to the mesoporous material (ref. 6) and R is the radius of the pore. The red and open dots correspond to the data for microporous zeosils (Table 1). In these latter cases, R is the largest cavity radius within the frameworks.[51] The dotted lines are guides to the eyes.

Fig. 13 Water intrusion–extrusion diagrams for (a) ZIF-8, (b) ZIF-67 and (c) ZIF-71. (b) and (c) data are shifted by 0.75 mL g^{-1} each along the y axis. Reproduced from ref. 73 with permission from The Royal Society of Chemistry.

that the Washburn equation was not able to describe the change in intrusion pressure with the inverse of the entrance pore radius of the frameworks. It turns out however, that such diagrams should better be sketched using the largest cavity radius of the framework[51] instead, provided that the intrusion process is an equilibrium transition. This is shown in Fig. 12 for the seven stable zeosils described above in Section 2.2.

From what was discussed in this section, it is tempting to differentiate between the zeosils with the largest cavity radii (AFI, DDR, MEL, MFI, red dots in Fig. 12) for which the intrusion pressure data fall approximately along a Washburn-like straight line, and the highly confining zeosils MTW, FER and TON (open dots in Fig. 12), for which the data seem to correspond to a different behavior. This is in keeping with the molecular simulation results described above: a first-order intrusion transition in the case of MFI and presumably also for AFI, DDR and MEL, and a supercritical behavior for the 3 other zeosils. This obviously deserves some more work in order to confirm that a classical Washburn-like model is still valid for pore radii as small as $\simeq 4$ Å.

The slope of the dotted lines in Fig. 12 are different, presumably because of the difference in chemistry of the porous walls. Hydrophobicity is generated in MCM-41 by covalent grafting of non polar organic chains, while the solid walls of zeosils are made of pure silica. Applying Washburn equation to these data, and using the macroscopic value of the water surface tension, we find that the apparent advancing contact angle (whatever this means in these highly confining systems) is $\simeq 120°$ in the mesoporous materials and $\simeq 100°$ in the zeosil materials.

2.4 Zeolite imidazolate frameworks (ZIFs) – water systems

Ortiz et al.[70] were the first to extend the water intrusion–extrusion experiments to other types of crystalline open-framework materials. Zeolite imidazolate frameworks (ZIFs) are a sub-class of metal–organic frameworks (MOFs) which possess zeolite-related frameworks with various topologies, but with higher
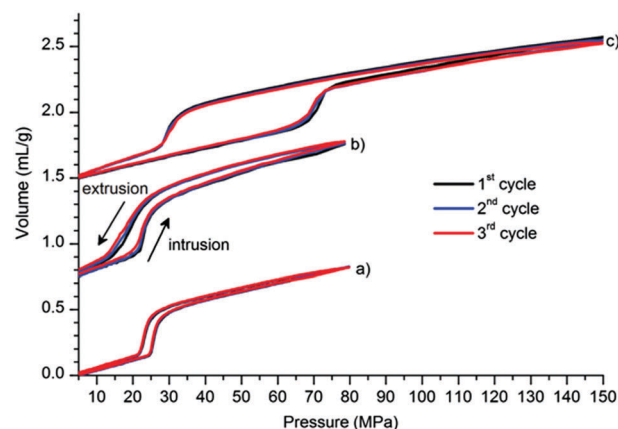
pore size and porous volume.[71] Depending on their topology, pore geometry and linker functionalization, the internal surface of the pores can either be hydrophilic or hydrophobic.[72] Khay et al[73] studied 8 different ZIFs having either the SOD or RHO topology. They found that ZIF-8, ZIF-67 and ZIF-71 exhibited high pressure liquid water intrusion. Grosu et al.[99] studied the temperature dependence of the water intrusion transition in ZIF-8.

As seen in Fig. 13, ZIF-8 and ZIF-67 (SOD topologies) display an intrusion transition at $\simeq 25$ MPa while the water intrusion pressure for ZIF-71 (RHO topology) is $\simeq 70$ MPa. These 3 ZIFs exhibit a Shock Absorber (SA) behavior, the transition hysteresis being larger in ZIF-71 than in the other two ZIFs. The stored energies are 10.8, 13.4 and 25.5 J g^{-1} for ZIF-8, 67 and 71 respectively, which in the latter case is the higher value observed among all the microporous materials studied so far (see Table 1 above for comparison). In addition, these 3 ZIF materials happen to be quite stable and resistant towards hydrolysis, as evidenced by the XRD analysis performed before and after several intrusion–extrusion cycles.[73–75]

Overall, hydrophobic ZIF materials seem to be very promising for energy storage applications.

2.5 Intrusion of electrolyte solutions

As a part of an important number of studies of the water infiltration–defiltration process in nanoporous materials,[10,76–82] Qiao and coworkers[83,84] demonstrated that water could no longer infiltrate (i.e. "be soaked up spontaneously") in a hydrophilic zeolite Y when an electrolyte was added. They related there finding to the increase of the aqueous solution surface tension. While it is generally assumed that cations are responsible for the change in surface tension with an increasing amount of electrolytes, Han et al.[84] showed that anions had also a strong effect in the confining nanoporous systems.

On account of the Washburn equation (Appendix, eqn (4)), an increase of the fluid interfacial tension should lead to an increase of the intrusion pressure. Patarin and coworkers[85,86]
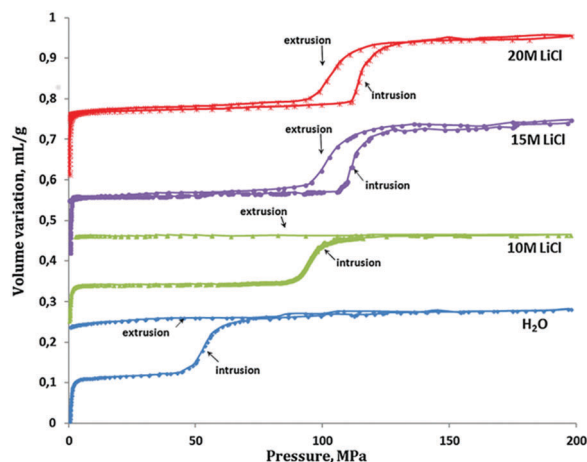
This journal is © The Royal Society of Chemistry 2017

Chem. Soc. Rev., 2017, **46**, 7421–7437 | **7429**

Fig. 14 Intrusion–extrusion process in the *BEA zeosil-aqueous solution systems. With pure water, *BEA behaves like a bumper. As the LiCl concentration increases, the intrusion pressure is enhanced and a change in behavior from bumper to shock-absorber is observed from 10 M to 15 M of LiCl. Reproduced from ref. 50 with permission from The Royal Society of Chemistry.
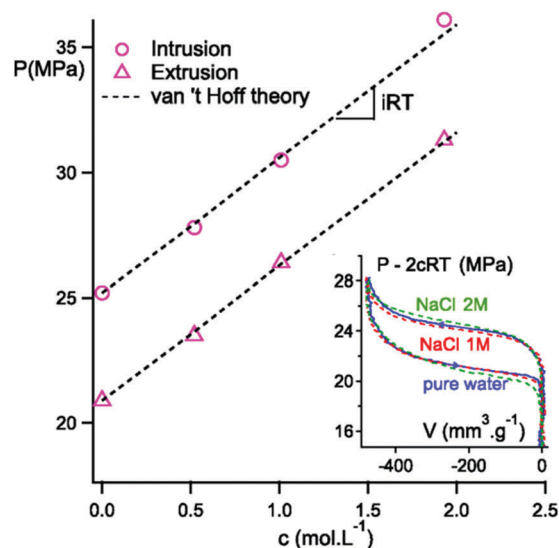

Fig. 15 Intrusion and extrusion pressures for NaCl solutions of various concentrations in ZIF-8 at 323 K. The inset displays intrusion–extrusion curves, plotted not in absolute pressure P but as a function of $P - 2cRT$, showing that the effect of concentration is well explained by the van 't Hoff osmotic pressure. Reproduced with permission from ref. 11. Copyright 2015 by the American Physical Society.

were the first to show that the intrusion pressure in silicalite-1 (MFI zeosil) was increased by a factor of $\simeq 3$ when using a concentrated solution of lithium chloride (LiCl, $3H_2O$), instead of pure water. Such an effect was also found in the case of NaCl and $MgCl_2$ solutions. Consequently the stored energy was also increased by the same factor, which seems very promising in view of potential energy storage applications. This has lead to a number of such aqueous solutions intrusion–extrusion studies in various zeosils as well as ZIF-8 materials.

In addition to the effect of increasing the intrusion pressure, the use of electrolyte solutions can lead to a drastic change in the intrusion–extrusion behavior. Ryzhikov et al.[50] showed that *BEA zeosil changed its behavior from bumper to shock-absorber, as the LiCl concentration increased from 10 M to 15 M. This is shown in Fig. 14. Structural analysis (XRD and NMR) showed that the *BEA framework was no more affected by the aqueous solution intrusion as far as silanol defects were concerned. This provided a further demonstration, after Section 2.2, that the bumper behavior of some zeosil–water systems is linked with an hydration phenomenon taking place during the high pressure intrusion–extrusion process. Everything occurs as if the use of an electrolyte aqueous solution protects the zeosil framework from hydration.

The same phenomenon was observed in the case of BEC zeosil–LiCl aqueous solution systems,[46] and to a certain extend to LTA zeosil.[48] In the case of CHA zeosil, the mixed shock-absorber-bumper behavior[40] turned into a pure shock-absorber behavior in presence of aqueous LiCl solutions.[87] Along these lines, it was also shown that weakly hydrophilic materials such as high Si/Al ratio zeolites[88] or COK-14 zeolites[89] could exhibit an intrusion transition in the presence of electrolyte aqueous solutions.

The ZIF-8-aqueous electrolyte solution system was investigated by Ortiz et al.[74] and Michelin-Jamois et al.[11] Several electrolyte

solutions were used. In all cases, as expected, the intrusion pressure was enhanced as the electrolyte concentration increased and the intrusion–extrusion cycles were shifted replicas of the pure water cycles. Only at high electrolyte concentration (4 M in sodium, lithium or potassium chloride) did the intrusion transition became sluggish and a small bumper behavior took place.[74] Based on the findings of a molecular dynamics study,[90] Michelin-Jamois suggested that only pure water was intruded in the material's pore. According to this hypothesis, the shift in intrusion pressure is due to the osmotic pressure, i.e. the difference in pressure between the pure water pressure inside the pore and the aqueous solution pressure outside the porous framework. A simple application of the van't Hoff osmotic equation ($\Pi = iCRT$) confirmed this model in most of the studied cases. These results are illustrated in Fig. 15. Also the data of Tzanis et al.[85] agreed with some previous molecular dynamics computation of the osmotic pressure of NaCl solutions.[91] Deviations from the van't Hoff law were observed in a few cases (NaI and LiI for instance) and this was tentatively attributed to some electrolyte intrusion in the framework.[11]

Despite the large number of intrusion experiments of electrolyte solutions in microporous materials, there was no direct evidence of the nature of the intruded liquid up to the work of Arletti et al.[92] For the first time intrusion–extrusion experiments of $MgCl_2$ aqueous solution were coupled to in situ high pressure synchrotron X-ray diffraction analysis. This study clearly demonstrated the presence of both ions and water molecules in the high pressure intruded liquid. A partial Mg^{2+} desolvation was observed and the intruded liquid composition was found to be more concentrated than the bulk liquid ($MgCl_2 \cdot 10H_2O$ instead of $MgCl_2 \cdot 21H_2O$). This seminal work opens up a new chapter of the study of the intrusion–extrusion phenomenon.

7430 | Chem. Soc. Rev., 2017, 46, 7421–7437

This journal is © The Royal Society of Chemistry 2017

An understanding of when and why ions in the aqueous solution enter the microporous frameworks will require further such studies, possibly augmented by molecular simulations.

Overall the replacement of pure water by electrolyte aqueous solutions seems to be very promising for future applications, given the observed enhancement of the intrusion pressure and the apparent gain in stability of the microporous frameworks with respect to hydration.

2.6 Energy storage device applications

As mentioned above in Section 2, Eroshenko was the first to investigate the possibility of storing mechanical energy by forced intrusion of a non wetting liquid in porous materials.[3,33,65] This was followed by Suciu and coworkers,[93–96] who studied the damping performances of the water-grafted silica gel system (which they called a colloidal damper), in order to determine how it could be designed to be used in practical applications such as vehicle suspensions, bumpers, engine supports, blast wave or intense impact mitigators,[97] etc.

The endurance tests performed by Suciu and Yaguchi[96] on a colloidal damper destined to vehicle suspension are particularly interesting. Water and silica gel particles were placed in a compression–decompression chamber located inside a high pressure cylinder. The tests were performed at the mean resonance frequency of usual suspensions, and with a pressurization of 100 MPa. The damping performances (dissipated energy and damping coefficient) were found to decrease slowly with the increasing number of working cycles, until a critical number of cycles was reached and then dropped abruptly. Two main reasons were invoked for the performance degradation. First of all the silica gel particles cracked into smaller parts as the number of compression–decompression cycles increases. This fatigue fracture effect is followed by a gradual leakage of the smallest silica pieces which migrate from the silica tank to the high pressure cylinder. To prevent the latter effect, a filter was introduced in the system in order to delay the inevitable particle leakage. Interestingly enough, the authors found that the critical cycles number increased from some $\simeq 10^3$ to $\simeq 10^6$ when using an appropriate filter with orifice diameter of a few μm. These are promising results given that the estimation of a vehicle damper durability is estimated to be $\simeq 10^7$.

More recently Chen and coworkers[8] studied the mechanical properties performance of a MFI–water molecular spring isolator. The stability of the zeosil framework was investigated through a 100 000 cycles sinusoidal test performed at 10 Hz using a standard piston–cylinder device. This test showed a very good stability of the zeosil after the endurance test, the force–displacement curve before and after the test being superimposable. This is very good news since no such endurance test with a large number of compression–decompression cycles using a zeosil material was ever performed before, to our best knowledge.

A fatigue fracture of the MFI particles was also observed, as in the above case of the silica gel particles. Chen mentioned that the design of the container was one of the issue to overcome.[8] The piston–cylinder structure faces the problem of sealing at high pressure. One must then find a zeosil with the right compromise between low enough intrusion pressure to tackle this issue, and a large intrusion pressure to store and release enough energy. On the other hand, the use of an electrolyte aqueous solution would enable to extend the working conditions of the damping system to temperatures lower than 0 °C.

Overall water–hydrophobic microporous materials are very promising energy storage systems. We have listed above in Sections 2.2 and 2.4 a certain number of zeosils and ZIF candidates for engineering applications, which we believe deserve in-depth studies through endurance tests similar to those reported above. It is also important to mention that water + silica (with perhaps a simple electrolyte such as NaCl) is an environmental friendly mixture.

2.7 Mechanical energy storage through pressure induced structural transitions in MOF materials

A sub-class of metal–organic framework (MOF) materials are called soft porous crystals[98] on account of their spectacular flexibility. The archetypical example of such highly flexible MOFs is the MIL-53 material designed and synthesized by Férey and coworkers.[99] MIL-53 displays the so-called breathing phenomenon, which consists of two successive crystal-to-crystal transformations upon simple gas adsorption, from a large pore (lp) state to a narrow pore (np) state, and back again to the lp state, the difference in unit cell volume between these two phases being of the order of 40%.[100] Neimark et al.[101] demonstrated that the internal adsorption stress which is responsible for the adsorption induced transitions is equivalent to the outside hydrostatic pressure needed to trigger the lp to np transition in the bare material. Indeed, Denoyel and coworkers were able for the first time to observe the pressure induced structural transition in MIL-53(Cr) using a mercury porosimeter, with a non penetrating pressure transmitting fluid.[23]

Denoyel and coworkers[23] noticed that the energy stored during this structural transition was comparable with the best hydrophobic silica discussed and reviewed in the present article (13.8 J g^{-1} in the case of MIL-53(Cr) for instance, see Table 1 for comparison). A few other studies confirmed that structural transitions in flexible MOFs such as MIL-47,[24] MIL-53-FA,[26] or DUT-49[102,103] were good candidates with respect to energy storage considerations, and this was confirmed by detailed thermodynamics analysis.[27,104] It turns out however that no studied MOF up to now exhibited a spring behavior with no dissipated energy.

3 Pressure-induced hydration (PIH) and pressure-induced phase transformations (PIPT)

In parallel with the presently reviewed physical chemistry studies of the high pressure water intrusion–extrusion phenomenon in hydrophobic microporous materials, there has been, over the years, an important amount of work dedicated to the properties of cationic hydrophilic zeolites under high pressure, mostly for geoscience purposes to start with.

This journal is © The Royal Society of Chemistry 2017

Chem. Soc. Rev., 2017, 46, 7421–7437 | 7431

This large area of research is somewhat out of the scope of the present review. Yet some of their findings are clearly related to our topic and very interesting links between these two areas have been disclosed recently. This is the subject of the present section.

Hazen investigated for the first time the effect of high pressure on zeolite 4A.[105] He was using a Diamond Anvil cell (DAC) (see Fig. 17) and found that the high pressure behavior of zeolite 4A was very much dependent on the pressure transmitting medium (PTM). Three distinct volume discontinuities, attributed to phase transitions, were observed when compressing the zeolite sample up to $\simeq 4$ GPa with a mixture of methanol and ethanol while no such discontinuities took place when using water instead. This was the beginning of a long list of studies highlighting the dependence of the high pressure behavior of zeolites and other microporous materials on the nature of the pressure-transmitting fluid.

Lee *et al.*[106] studied the high pressure behavior of zeolite natrolite using a DAC together with synchrotron XRD. Piermarini *et al.*[107] have shown that a liquid mixture 4 : 1 in volume of methanol and ethanol remained hydrostatic in a DAC experiment to almost 10 GPa at room temperature. In this work, and in many of the following ones on the same subject, Lee *et al.* used a mixture of 16 : 3 : 1 by volume of methanol, ethanol and water (m.e.w.) respectively as the PTM. Such a mixture is close to the Piermarini recipe which guarantees hydrostaticity at very high pressure while introducing a small quantity of water in the PTM that will have a pronounced effect on the high pressure behavior of the studied zeolites. Indeed the authors observed an abrupt volume expansion around 1.5 GPa upon pressure increase in the natrolite sample.[106] Rietveld analysis showed that it corresponded to a selective intrusion of water from the PTM into the zeolite porous volume. This gave rise to a so-called super-hydrated phase of natrolite in which the amount of structural water was doubled as compared to the ambient pressure phase. The pressure induced swelling was accompanied by a change in the crystal structure and a relocation of the water molecules within the framework.

The pressure-induced hydration (PIH) process in natrolite was found to be reversible and the initial phase was recovered upon pressure release. Interestingly enough, for the closely related potassium gallosilicate natrolite, PIH was found to be irreversible, with a retention of the high pressure phase at ambient conditions.[108,109] This opens the route to the discovery of new materials with new properties. The quest for confinement-induced organized nanostructures using external stimuli such as light or electric field now includes the use of high pressure. Recently Arletti *et al.*[110] have observed a spectacular organization of ethanol and water molecules in FER zeosil upon compression at 0.84 GPa. Ethanol and water molecules are extracted from the PTM and form 2D networks of ethanol dimers and cyclic water tetramers. Ethanol and water molecules are segregated in different channels of the FER zeosil. This supramolecular structure remains stable upon pressure release. Further studies are expected in the future along these lines. A combination of microporous organized frameworks with high pressure
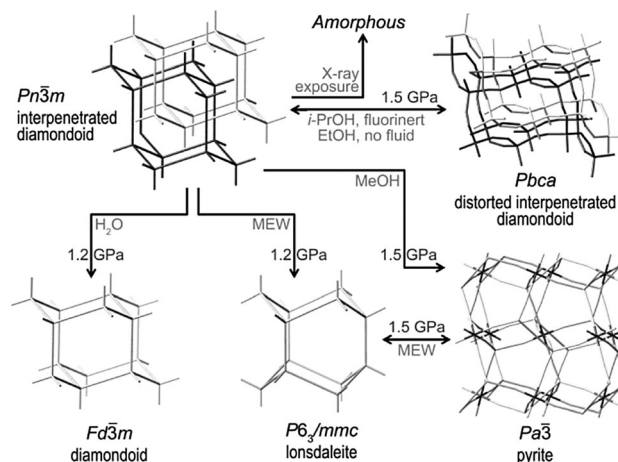

Fig. 16 Summary of the various phases formed upon compression of $Zn(CN)_2$ in different fluid media. The ambient phase is nonporous and has an interpenetrated diamondoid net. Upon compression in water, methanol, and m.e.w. (methanol–ethanol–water mixture) it transforms into a noninterpenetrated diamondoid, pyrite, and lonsdaleite net respectively. Reproduced with permission from ref. 32. Copyright 2013 American Chemical Society.

insertion of molecular species are expected to lead to the discovery of new nanocomposites.

New materials may also be obtained at high pressure using a non-penetrating fluid (usually a silicon oil). Jordá *et al.*[111] found that a phase transition was taking place in ITQ-29 zeosil at 3.2 GPa, leading irreversibly to a new material called ITQ-50. A most remarkable result was obtained by Chapman and coworkers[32] who showed that stable porous polymorphs of $Zn(CN)_2$ could be generated irreversibly upon compression at 2 GPa of an initially non porous sample (1.5 to 2 GPa). The different resulting phases being obtained using different PTM are represented in Fig. 16. Structural transitions or amorphization in MOFs and ZIFs materials are also currently subject to an intense research effort.[28–32,112]

In addition to the materials described above in this chapter, the structural behavior of several other zeolites under high pressure was investigated in the past decade, highlighting the presence or absence of PIH depending on the PTM used, and other unusual structural behavior. It turns out that the link between these studies of scolectite,[113] bikitaite,[114] gismondine,[115,116] dealuminated Y[117] and others, on the one hand, and the aqueous solutions intrusion–extrusion in zeosils is not obvious for at least two reasons. First of all, the zeolitic materials are cationic hydrophilic in the PIH studies while they are hydrophobic in the water intrusion work. The insertion of water molecules in the first case has to do with structural water, some of those being already present initially in some specific sites in the porous framework, accompanied by some rearrangement of the extraframework cations. In the second case the zeosil framework does not contain any cation or structural water initially (at least in the ideal case of a purely hydrophobic material). Water intrusion has to do with filling the porous network with bulk water, to put it in a straightforward way.
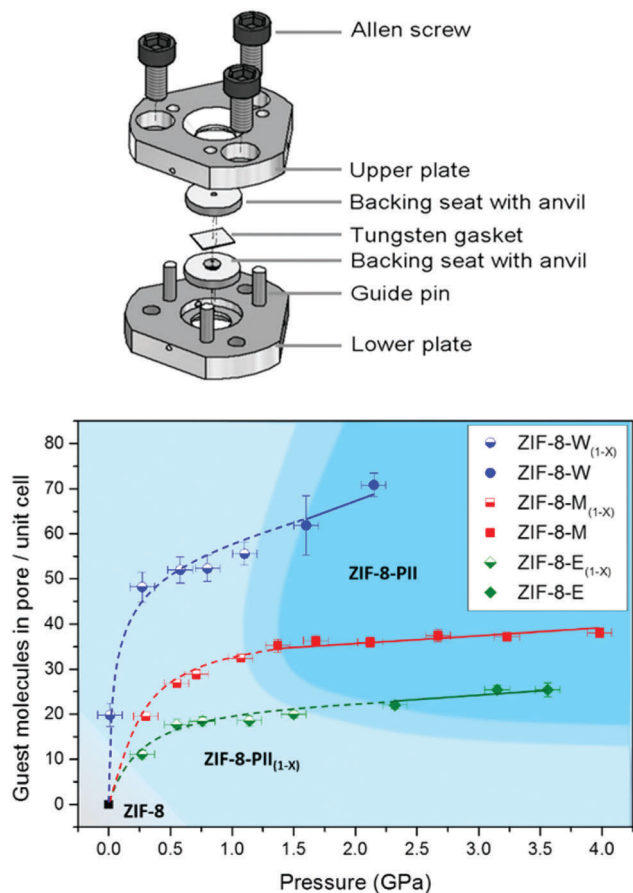
Fig. 17 Top: Schematic of a modified Merrill–Bassett diamond–anvil cell (DAC) used in high-pressure single-crystal X-ray diffraction experiments.[119] Bottom: Pressure-induced insertion of guest molecules into the pores of ZIF-8, using water (W), methanol (M), and ethanol (E) as pressure-transmitting fluids. The uptake was determined by the residual electron density derived from Rietveld refinements of X-ray powder diffraction.[120] For water, 100 molecules per unit cell corresponds to 7.91 mL g^{-1}. For ethanol, 20 molecule per unit cell is 4.04 mL g^{-1}. For methanol, 40 molecules per unit cell is 5.62 mL g^{-1}. Top: Reproduced from ref. 119 with permission of the International Union of Crystallography. Bottom: Reproduced with permission from ref. 120. Copyright 2016 by the American Physical Society.

The second reason stems from the methodologies used in both cases. High pressure of the order of 1–10 GPa and *in situ* XRD structural analysis in the first case. Much lower pressure of the order of 0.1–0.2 GPa and thermodynamic data acquisition only in the second case.

It is nonetheless tempting to bring these two phenomena closer to each other. This was first attempted recently by Arletti *et al.*[118] who investigated both the cationic Monastir ferrierite (Mon-FER) and the all-silica ferrierite zeosil, using the DAC/XRD methodology and both types of PTM, namely the standard 16 : 3 : 1 methanol–ethanol–water mixture (m.e.w.) and the non penetrating silicone oil fluid. Unfortunately the quality of the XRD data were insufficient to show whether or not PIH took place in the Mon-FER sample. On the other hand they clearly showed that 15 water molecules per unit cell were present in the all-silica zeosil at 0.2 GPa, using the m.e.w. PTM. This is in very good agreement with the porosimetry experiment shown

above in Fig. 8. In addition the structural XRD analysis showed that water was mainly existing as bulk-like and 1D clusters, in agreement with molecular simulations,[7,53] but this was the first direct *in situ* observation. Recently Arletti *et al.*[92] combined aqueous water solution porosimetry and DAC/XRD experiments in order to demonstrate that some of the ions of the electrolyte solution were effectively intruded into the porous framework (see Section 2.5 above). Obviously the scientific areas corresponding to aqueous water intrusion and PIH/PIPT have much to share, from both the conceptual and the experimental practical sides.

Finally, it is worth noting that have recently been a significant number of studies of the behavior of MOFs at high pressure, using pressure-transmitting fluids that range from non-penetrating silicon oils to smaller molecules such as water and short alcohols. This topic was recently reviewed in detail by McKellar and Moggach.[119] As mentioned above in the case of zeolites, the current direction of research is to couple the understanding of pressure-induced deformation and the uptake of fluid molecules insides the pores. We give an example in Fig. 17 (bottom panel) of a recent study that achieved this by quantifying the uptake inside the pores by calculating the residual electron density derived from Rietveld refinements of X-ray powder diffraction. The authors show the impact of host–guest molecular interactions as the structural changes of ZIF-8 observed under pressure are guest-dependent, as well as influence the pressure at which the material becomes amorphous.

4 Conclusion and future prospects

Since the seminal article of Patarin and coworkers in 2001,[4] in which the high pressure water intrusion–extrusion phenomenon in zeosil materials was reported for the first time, a new field of research has progressively emerged and is now very active. A series of at least seven zeosil frameworks namely AFI, DDR, MEL, MFI, MTW, FER and TON, were found suitable for reversible energy storage because of their stability with respect to hydrolysis after several water intrusion–extrusion cycles. Three microporous hydrophobic zeolite imidazolate frameworks (ZIFs), namely ZIF-8, ZIF-67 and ZIF-71 also happen to be quite stable and resistant towards hydrolysis, as evidenced by the XRD analysis performed before and after several intrusion–extrusion cycles, and thus seem very promising for energy storage applications.

The energy stored accompanying water intrusion lie in the range 3 to 15 J g^{-1} for the zeosil materials, and increases up to 25 J g^{-1} for ZIF-71. This is in the same range as organic elastomers (of the order of 20 J g^{-1}) and significantly higher than torsion or plate springs (typically 20 J g^{-1}).[121] Replacing pure water by electrolyte aqueous solutions enables to increase the stored energy by a factor close to 3, on account of the high pressure shift of the intrusion transition. It is also interesting to mention that the use of an electrolyte aqueous solution seems to protect the zeosil framework from hydration. In addition to the fact that aqueous solutions and microporous silica materials are environmental friendly, these systems are thus

This journal is © The Royal Society of Chemistry 2017

Chem. Soc. Rev., 2017, **46**, 7421–7437 | 7433

becoming increasingly interesting for the design of new energy storage devices. The need exists to extend the endurance tests to such materials as ZIFs, and also using electrolyte solutions.

From a fundamental point of view, understanding the behavior of confined water in hydrophobic cavities has made some progress. Molecular simulation studies showed that water condensation (*i.e.* capillary evaporation) takes place through a genuine first-order phase transition, provided that the interconnected pores structure is 3-dimensional and sufficiently open. In an extreme confinement situations such as in FER zeosil, condensation seem to take place through a continuous supercritical crossing from a diluted to a dense fluid, on account of the fact that the first-order transition line is shifted to higher pressure, and the confined water critical point is correlatively shifted to lower temperature. These molecular simulation studies suggest that the most important features of the intrusion/extrusion process can be understood in terms of equilibrium thermodynamics considerations. More work is certainly needed to confirm these points and to extend the simulations to electrolyte aqueous solutions and ZIF materials.

Several questions remain unanswered and important issues need to be tackled in future works. To start with, the new chapter of the intrusion of electrolyte aqueous solutions needs some further investigations in order to understand what is the intrusion mechanism in presence of a fluid mixture and what actually determines the fact that ionic species do or do not penetrate inside the porous framework. Coupling porosimetry and thermodynamic experiments with molecular simulations has been successful and should be extended to the electrolyte solution issue. DAC/XRD *in situ* experiments will of course be needed as well.

More generally, a combination of porosimetry, DAC/XRD experiments and molecular simulations is certainly desirable in order to address the most difficult issues. There is still much to understand in the pressure-induced hydration (PIH), pressure-induced phase transformation (PIPT) and pressure-induced irreversible segregation and supramolecular ordering phenomena, to name a few. For instance, it is not clear why water and ethanol can both penetrate the FER zeosil framework when using a binary water–ethanol mixture as the PTM,[110] while only water molecules seem to penetrate into the same zeosil when using the standard m.e.w. solution as the PTM[118] In the case of PIH in cationic zeolites, water molecules are expected to penetrate at very low pressure (*i.e.* below the saturation vapor pressure) on account of the hydrophilic nature of the framework.[54] If so, the hydration process would take place with the porous volumes fully saturated with water molecules. Then why does this happen at such a high pressure (1.5 GPa)? This needs to be tested in order to better understand pressure-induced hydration.

In real life ''hydrophobic'' surfaces are geometrically, chemically and electrically heterogeneous objects.[122] Pure graphite surfaces for instance are believed to be hydrophobic, but nanoporous activated carbons exhibit a various amount of local functionalization of the pore surface (hydrophilic oxygenated sites). This is known to have a strong effect on the water uptake in porous carbon materials.[123–126] The fundamental question is thus: "How does confined water behave in response to

heterogeneous surfaces?".[39] This question is common to a wide variety of nanoporous media, from biological cavities and porous polymers to inorganic materials such as porous carbons, zeolites, micelle-templated materials and other open framework porous materials. In addition to the experimental methodologies reviewed in the present article, extended osmotic molecular simulations will be needed in order to take into account the deformation of the framework materials upon fluid intrusion.

Conflicts of interest

There are no conflicts to declare.

Appendix: thermodynamics of confined fluids

In nanoporous materials, fluids are confined to spaces of dimensions comparable to the range of intermolecular interactions. Their physico-chemical behavior can then be markedly altered compared with its corresponding bulk counterpart.

Let us consider a simple model in which a fluid is confined between two parallel walls of area A, separated by a distance h (see Fig. 18). The fluid in this slit-pore system is in contact with a fluid reservoir at constant chemical potential μ and temperature T. The appropriate thermodynamic potential for this open system is the grand potential Ω, the exact differential of which writes:[127,128]

$$\mathrm{d}\Omega = -p\mathrm{d}V - S\mathrm{d}T - N\mathrm{d}\mu + 2\gamma\mathrm{d}A - Ap_{\mathrm{solv}}\mathrm{d}h \qquad (1)$$

where p is the bulk pressure, V the volume occupied by the confined fluid, S its entropy and N the number of molecules adsorbed in the slit-pore. The first three terms correspond to the bulk fluid and the last two terms represent the effect of the two additional thermodynamic fields, A and h that originate from the confining geometry. The first of these two terms is the interfacial term, in which γ is the wall–fluid interfacial tension, and the second one is a specific confinement term, with:

$$p_{\mathrm{solv}} = p(h) - p_{\mathrm{bulk}} = -\frac{1}{A}\left(\frac{\partial \Omega}{\partial h}\right)_{\mu, T, A} \qquad (2)$$

where $p(h)$ is the pressure exerted on the pore walls by the confined fluid. P_{solv} is called the solvation pressure.[127–129]
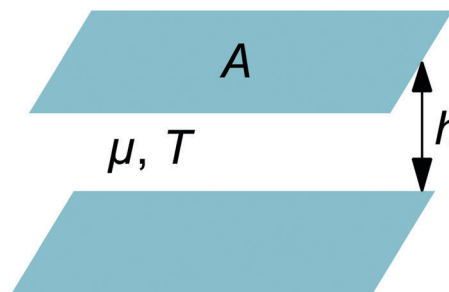

Fig. 18   The slit-pore model of a fluid confined between two parallel walls.

In the limit of $h \to \infty$ the solvation pressure vanishes, while in highly confined systems structured fluid density profiles (layering) causes the solvation pressure to oscillate, as observed in the surface force apparatus (SFA) experiments[130–132] and simulations[133–135] for system geometries similar to the slit-pore situation in which layered structure take place. In more complex and realistic systems, with corrugated surfaces for instance, there are some evidences that the solvation pressure oscillation is much less pronounced.[136,137]

As noted by Evans,[128] the presence of two additional thermodynamic fields has significant repercussions for phase equilibrium. They may augment the Gibbs phase rule leading to a richer phase diagram for a single component fluid.[127]

Capillary condensation takes place in a pore of width h at a chemical potential $\mu < \mu_{\mathrm{sat}}$ (or equivalently at a pressure $p < p_{\mathrm{sat}}$). In the limit of large pore width, the undersaturation at which vapor condensation takes place is described thermodynamically by the Kelvin equation:[1]

$$\ln\left(\frac{p}{p_{\mathrm{sat}}}\right) = -\frac{2\gamma_{\mathrm{LV}}\cos\theta}{RT\rho_{\mathrm{L}}h} \qquad (3)$$

where γ_{LV} is the liquid–vapor interfacial tension, θ is the fluid–solid contact angle and ρ_{L} is the liquid density.

For a wetting fluid ($\cos\theta > 0$) condensation occurs for $p < p_{\mathrm{sat}}$. For $\cos\theta < 0$, eqn (3) predicts capillary evaporation for some $p > p_{\mathrm{sat}}$ and this is relevant for the study of the intrusion process of non wetting fluid in porous materials. Along this line, Porcheron et al.[35] demonstrated the thermodynamic equivalence between capillary condensation of a wetting fluid and forced intrusion of a non wetting fluid.

Mercury porosimetry has long been used to characterize macroporous materials,[2] and the porosimetry equipment has been further adapted and is now used more and more to study water intrusion in hydrophobic nanoporous solids. A convenient way to relate the pore width h with the hydraulic pressure p that must be applied to the non wetting liquid to penetrate the pore is to use the approximate Washburn equation:[138]

$$p = -\frac{2\gamma_{\mathrm{LV}}\cos\theta_{\mathrm{a}}}{h} \qquad (4)$$

where θ_{a} is the advancing contact angle adopted by the triple line during the intrusion process.[6]

References

1 J. Rouquerol, F. Rouquerol, P. Llewellyn, G. Maurin and K. S. W. Sing, Adsorption by Powders and Porous Solids: Principles, Methodology and Applications, Academic Press, 2013.

2 J. Rouquerol, G. Baron, R. Denoyel, H. Giesche, J. Groen, P. Klobes, P. Levitz, A. V. Neimark, S. Rigby, R. Skudas, K. Sing, M. Thommes and K. Unger, Pure Appl. Chem., 2011, 84, 107–136.

3 A. Y. Fadeev and V. A. Eroshenko, J. Colloid Interface Sci., 1997, 187, 275–282.

4 V. Eroshenko, R.-C. Regis, M. Soulard and J. Patarin, J. Am. Chem. Soc., 2001, 123, 8129–8130.

5 V. Eroshenko, R.-C. Regis, M. Soulard and J. Patarin, C. R. Phys., 2002, 3, 111–119.

6 B. Lefevre, A. Saugey, J. L. Barrat, L. Bocquet, E. Charlaix, P. F. Gobin and G. Vigier, J. Chem. Phys., 2004, 120, 4927–4938.

7 N. Desbiens, I. Demachy, A. H. Fuchs, H. Kirsch-Rodeschini, M. Soulard and J. Patarin, Angew. Chem., Int. Ed., 2005, 44, 5310–5313.

8 M. Yu, X. Gao and Q. Chen, Noise Control, 2016, 2016, 1–10.

9 Y. Grosu, V. Eroshenko, J. M. Nedelec and J. P. E. Grolier, Phys. Chem. Chem. Phys., 2015, 17, 1572–1574.

10 L. Liu, X. Chen, W. Lu, A. Han and Y. Qiao, Phys. Rev. Lett., 2009, 102, 184501.

11 M. Michelin-Jamois, C. Picard, G. Vigier and E. Charlaix, Phys. Rev. Lett., 2015, 115, 036101.

12 P. Ball, Nature, 2003, 423, 25–26.

13 D. Chandler, Nature, 2002, 417, 491.

14 N. Giovambattista, P. J. Rossky and P. G. Debenedetti, Phys. Rev. E: Stat., Nonlinear, Soft Matter Phys., 2006, 73, 2671.

15 A. C. Fogarty, F.-X. Coudert, A. Boutin and D. Laage, ChemPhysChem, 2014, 15, 521–529.

16 D. Takaiwa, I. Hatano, K. Koga and H. Tanaka, Proc. Natl. Acad. Sci. U. S. A., 2008, 105, 39–43.

17 J. Stelzer, M. Paulus, M. Hunger and J. Weitkamp, Microporous Mesoporous Mater., 1998, 22, 1–8.

18 R. N. Eissmann and M. D. L. Van, Ind. Eng. Chem. Res., 1993, 32, 2752–2757.

19 M. Wikström, Curr. Opin. Struct. Biol., 1998, 8, 480–488.

20 O. Beckstein and M. S. P. Sansom, Proc. Natl. Acad. Sci. U. S. A., 2003, 100, 7063–7068.

21 M. D. Collins, G. Hummer, M. L. Quillin, B. W. Matthews and S. M. Gruner, Proc. Natl. Acad. Sci. U. S. A., 2005, 102, 16668–16671.

22 B. Pereira, S. Jain and S. Garde, J. Chem. Phys., 2006, 124, 074704.

23 I. Beurroies, M. Boulhout, P. L. Llewellyn, B. Kuchta, G. Férey, C. Serre and R. Denoyel, Angew. Chem., Int. Ed., 2010, 49, 7526–7529.

24 P. G. Yot, Q. Ma, J. Haines, Q. Yang, A. Ghoufi, T. Devic, C. Serre, V. Dmitriev, G. Férey, C. Zhong and G. Maurin, Chem. Sci., 2012, 3, 1100.

25 P. G. Yot, Z. Boudene, J. Macia, D. Granier, L. Vanduyfhuys, T. Verstraelen, V. V. Speybroeck, T. Devic, C. Serre, G. Férey, N. Stock and G. Maurin, Chem. Commun., 2014, 50, 9462–9464.

26 P. G. Yot, L. Vanduyfhuys, E. Alvarez, J. Rodriguez, J.-P. Itié, P. Fabry, N. Guillou, T. Devic, I. Beurroies, P. L. Llewellyn, V. V. Speybroeck, C. Serre and G. Maurin, Chem. Sci., 2016, 7, 446–450.

27 J. Rodriguez, I. Beurroies, M.-V. Coulet, P. Fabry, T. Devic, C. Serre, R. Denoyel and P. L. Llewellyn, Dalton Trans., 2016, 45, 4274–4282.

28 S. Moggach, T. Bennett and A. Cheetham, Angew. Chem., Int. Ed., 2009, 48, 7087–7089.

This journal is © The Royal Society of Chemistry 2017

Chem. Soc. Rev., 2017, 46, 7421–7437 | 7435

29 T. D. Bennett, P. Simoncic, S. A. Moggach, F. Gozzo, P. Macchi, D. A. Keen, J.-C. Tan and A. K. Cheetham, *Chem. Commun.*, 2011, **47**, 7983.

30 E. C. Spencer, M. S. R. N. Kiran, W. Li, U. Ramamurty, N. L. Ross and A. K. Cheetham, *Angew. Chem., Int. Ed.*, 2014, **53**, 5583–5586.

31 M. T. Wharmby, S. Henke, T. D. Bennett, S. R. Bajpe, I. Schwedler, S. P. Thompson, F. Gozzo, P. Simoncic, C. Mellot-Draznieks, H. Tao, Y. Yue and A. K. Cheetham, *Angew. Chem., Int. Ed.*, 2015, **54**, 6447–6451.

32 S. H. Lapidus, G. J. Halder, P. J. Chupas and K. W. Chapman, *J. Am. Chem. Soc.*, 2013, **135**, 7621–7628.

33 V. Eroshenko, *WO Pat.*, 018 040, 1996; V. Eroshenko, *WO Pat.*, 01/55616, 2001.

34 M. Thommes, K. Kaneko, A. V. Neimark, J. P. Olivier, F. Rodriguez-Reinoso, J. Rouquerol and K. S. Sing, *Pure Appl. Chem.*, 2015, **87**, 1051–1069.

35 F. Porcheron, P. A. Monson and M. Thommes, *Langmuir*, 2004, **20**, 6482–6489.

36 E. M. Flanigen, J. M. Bennett, R. W. Grose, J. P. Cohen, R. L. Patton, R. M. Kirchner and J. V. Smith, *Nature*, 1978, **271**, 512–516.

37 J. Guth, H. Kessler and R. Wey, *Studies in Surface Science and Catalysis*, Elsevier, 1986, pp. 121–128.

38 M. Trzpit, M. Soulard, J. Patarin, N. Desbiens, F. Cailliez, A. Boutin, I. Demachy and A. H. Fuchs, *Langmuir*, 2007, **23**, 10131–10139.

39 F. Cailliez, G. Stirnemann, A. Boutin, I. Demachy and A. H. Fuchs, *J. Phys. Chem. C*, 2008, **112**, 10435–10445.

40 M. Trzpit, S. Rigolet, J.-L. Paillaud, C. Marichal, M. Soulard and J. Patarin, *J. Phys. Chem. B*, 2008, **112**, 7257–7266.

41 F. Cailliez, M. Trzpit, M. Soulard, I. Demachy, A. Boutin, J. Patarin and A. H. Fuchs, *Phys. Chem. Chem. Phys.*, 2008, **10**, 4817.

42 L. Tzanis, M. Trzpit, M. Soulard and J. Patarin, *Microporous Mesoporous Mater.*, 2011, **146**, 119–126.

43 L. Tzanis, M. Trzpit, M. Soulard and J. Patarin, *J. Phys. Chem. C*, 2012, **116**, 4802–4808.

44 L. Tzanis, M. Trzpit, M. Soulard and J. Patarin, *J. Phys. Chem. C*, 2012, **116**, 20389–20395.

45 L. Tzanis, B. Marler, H. Gies and J. Patarin, *J. Phys. Chem. C*, 2013, **117**, 4098–4103.

46 L. Ronchi, A. Ryzhikov, H. Nouali, T. J. Daou, S. Albrecht and J. Patarin, *Microporous Mesoporous Mater.*, 2017, **254**, 153–159.

47 M. Soulard, J. Patarin, V. Eroshenko and R. Regis, *Recent Advances in the Science and Technology of Zeolites and Related Materials Part B, Proceedings of the 14th International Zeolite Conference*, Elsevier, 2004, pp. 1830–1837.

48 A. Ryzhikov, L. Ronchi, H. Nouali, T. J. Daou, J.-L. Paillaud and J. Patarin, *J. Phys. Chem. C*, 2015, **119**, 28319–28325.

49 M. A. Saada, M. Soulard, B. Marler, H. Gies and J. Patarin, *J. Phys. Chem. C*, 2011, **115**, 425–430.

50 A. Ryzhikov, I. Khay, H. Nouali, T. J. Daou and J. Patarin, *Phys. Chem. Chem. Phys.*, 2014, **16**, 17893.

51 C. Baerlocher, W. M. Meier and D. H. Olson, *Atlas of Zeolite Framework Types*, Elsevier, 2001.

52 Y. G. Bushuev and G. Sastre, *J. Phys. Chem. C*, 2011, **115**, 21942–21953.

53 N. Desbiens, A. Boutin and I. Demachy, *J. Phys. Chem. B*, 2005, **109**, 24071–24076.

54 A. D. Lella, N. Desbiens, A. Boutin, I. Demachy, P. Ungerer, J.-P. Bellat and A. H. Fuchs, *Phys. Chem. Chem. Phys.*, 2006, **8**, 5396.

55 I. Brovchenko, A. Geiger and A. Oleinikova, *J. Chem. Phys.*, 2004, **120**, 1958–1972.

56 S. Sacquin, M. Schoen and A. H. Fuchs, *J. Chem. Phys.*, 2003, **118**, 1453–1465.

57 R. Radhakrishnan and K. E. Gubbins, *Phys. Rev. Lett.*, 1997, **79**, 2847–2850.

58 C. Bichara, J. Y. Raty and R. J.-M. Pellenq, *Phys. Rev. Lett.*, 2002, **89**, 016101.

59 C. Bichara, J.-Y. Raty and R. Pellenq, *Mol. Simul.*, 2004, **30**, 601–606.

60 K. Koga, G. Gao, H. Tanaka and X. Zeng, *Phys. A*, 2002, **314**, 462–469.

61 E. Braun, J. J. Chen, S. K. Schnell, L.-C. Lin, J. A. Reimer and B. Smit, *Angew. Chem., Int. Ed.*, 2015, **54**, 14349–14352.

62 L. Sarkisov, T. Düren and R. Q. Snurr, *Mol. Phys.*, 2004, **102**, 211–221.

63 K. S. Walton, A. R. Millward, D. Dubbeldam, H. Frost, J. J. Low, O. M. Yaghi and R. Q. Snurr, *J. Am. Chem. Soc.*, 2008, **130**, 406–407.

64 M. de Toni, P. Pullumbi, F.-X. Coudert and A. H. Fuchs, *J. Phys. Chem. C*, 2010, **114**, 21631–21637.

65 L. Coiffard, V. A. Eroshenko and J.-P. E. Grolier, *AIChE J.*, 2005, **51**, 1246–1257.

66 F. Porcheron, M. Thommes, R. Ahmad and P. A. Monson, *Langmuir*, 2007, **23**, 3372–3380.

67 T. Karbowiak, C. Paulin, A. Ballandras, G. Weber and J.-P. Bellat, *J. Am. Chem. Soc.*, 2009, **131**, 9898–9899.

68 T. Karbowiak, C. Paulin and J.-P. Bellat, *Microporous Mesoporous Mater.*, 2010, **134**, 8–15.

69 T. Karbowiak, G. Weber and J.-P. Bellat, *Langmuir*, 2014, **30**, 213–219.

70 G. Ortiz, H. Nouali, C. Marichal, G. Chaplais and J. Patarin, *Phys. Chem. Chem. Phys.*, 2013, **15**, 4888.

71 R. Banerjee, A. Phan, B. Wang, C. Knobler, H. Furukawa, M. OKeeffe and O. M. Yaghi, *Science*, 2008, **319**, 939–943.

72 A. U. Ortiz, A. P. Freitas, A. Boutin, A. H. Fuchs and F.-X. Coudert, *Phys. Chem. Chem. Phys.*, 2014, **16**, 9940–9949.

73 I. Khay, G. Chaplais, H. Nouali, G. Ortiz, C. Marichal and J. Patarin, *Dalton Trans.*, 2016, **45**, 4392–4400.

74 G. Ortiz, H. Nouali, C. Marichal, G. Chaplais and J. Patarin, *J. Phys. Chem. C*, 2014, **118**, 7321–7328.

75 G. Ortiz, H. Nouali, C. Marichal, G. Chaplais and J. Patarin, *J. Phys. Chem. C*, 2014, **118**, 21316–21322.

76 A. Han and Y. Qiao, *Chem. Lett.*, 2007, **36**, 882–883.

77 F. Surani, A. Han and Y. Qiao, *J. Mater. Res.*, 2006, **21**, 2389–2392.

78 X. Kong and Y. Qiao, *Philos. Mag. Lett.*, 2005, **85**, 331–337.

79 A. Han and Y. Qiao, *J. Am. Chem. Soc.*, 2006, **128**, 10348–10349.

80 A. Han, X. Kong and Y. Qiao, *J. Appl. Phys.*, 2006, **100**, 014308.

7436 | *Chem. Soc. Rev.*, 2017, **46**, 7421–7437

This journal is © The Royal Society of Chemistry 2017

81 A. Han, V. K. Punyamurtula and Y. Qiao, *Appl. Phys. Lett.*, 2008, **92**, 153117.

82 L. Liu, X. Chen, T. Kim, A. Han and Y. Qiao, *New J. Phys.*, 2010, **12**, 033021.

83 X. Kong, F. B. Surani and Y. Qiao, *Phys. Scr.*, 2006, **74**, 531–534.

84 A. Han, W. Lu, T. Kim, X. Chen and Y. Qiao, *Phys. Rev. E: Stat., Nonlinear, Soft Matter Phys.*, 2008, **78**, 031408.

85 L. Tzanis, H. Nouali, T. J. Daou, M. Soulard and J. Patarin, *Mater. Lett.*, 2014, **115**, 229–232.

86 I. Khay, T. J. Daou, H. Nouali, A. Ryzhikov, S. Rigolet and J. Patarin, *J. Phys. Chem. C*, 2014, **118**, 3935–3941.

87 L. Ronchi, A. Ryzhikov, H. Nouali, T. J. Daou and J. Patarin, *New J. Chem.*, 2017, **41**, 2586–2592.

88 A. Ryzhikov, I. Khay, H. Nouali, T. Daou and J. Patarin, *Microporous Mesoporous Mater.*, 2016, **221**, 1–7.

89 C. E. A. Kirschhock, M. D. Prins, E. Verheijen, A. Ryzhikov, T. J. Daou, H. Nouali, F. Taulelle, J. A. Martens and J. Patarin, *Phys. Chem. Chem. Phys.*, 2016, **18**, 18795–18801.

90 Z. Hu, Y. Chen and J. Jiang, *J. Chem. Phys.*, 2011, **134**, 134705.

91 Y. Luo and B. Roux, *J. Phys. Chem. Lett.*, 2010, **1**, 183–189.

92 R. Arletti, L. Ronchi, S. Quartieri, G. Vezzalini, A. Ryzhikov, H. Nouali, T. J. Daou and J. Patarin, *Microporous Mesoporous Mater.*, 2016, **235**, 253–260.

93 C. Suciu, T. Iwatsubo and S. Deki, *J. Colloid Interface Sci.*, 2003, **259**, 62–80.

94 C. V. Suciu, T. Iwatsubo and S. Deki, *JSME Int. J., Ser. C*, 2004, **47**, 180–188.

95 C. V. Suciu, T. Iwatsubo, K. Yaguchi and M. Ikenaga, *Computational Technologies for Fluid/Thermal/Structural/Chemical Systems With Industrial Applications*, 2004, vol. 1, pp. 211–221.

96 C. V. Suciu and K. Yaguchi, *Exp. Mech.*, 2008, **49**, 383–393.

97 B. Xu, Y. Qiao and X. Chen, *J. Mech. Phys. Solids*, 2014, **62**, 194–208.

98 S. Horike, S. Shimomura and S. Kitagawa, *Nat. Chem.*, 2009, **1**, 695–704.

99 G. Férey and C. Serre, *Chem. Soc. Rev.*, 2009, **38**, 1380.

100 C. Serre, S. Bourrelly, A. Vimont, N. Ramsahye, G. Maurin, P. Llewellyn, M. Daturi, Y. Filinchuk, O. Leynaud, P. Barnes and G. Férey, *Adv. Mater.*, 2007, **19**, 2246–2251.

101 A. V. Neimark, F.-X. Coudert, C. Triguero, A. Boutin, A. H. Fuchs, I. Beurroies and R. Denoyel, *Langmuir*, 2011, **27**, 4734–4741.

102 U. Stoeck, S. Krause, V. Bon, I. Senkovska and S. Kaskel, *Chem. Commun.*, 2012, **48**, 10841.

103 S. Krause, V. Bon, I. Senkovska, U. Stoeck, D. Wallacher, D. M. Többens, S. Zander, R. S. Pillai, G. Maurin, F.-X. Coudert and S. Kaskel, *Nature*, 2016, **532**, 348–352.

104 J. Rodriguez, I. Beurroies, T. Loiseau, R. Denoyel and P. L. Llewellyn, *Angew. Chem., Int. Ed.*, 2015, **54**, 4626–4630.

105 R. M. Hazen, *Science*, 1983, **219**, 1065–1067.

106 Y. Lee, J. A. Hriljac, T. Vogt, J. B. Parise and G. Artioli, *J. Am. Chem. Soc.*, 2001, **123**, 12732–12733.

107 G. J. Piermarini, S. Block and J. Barnett, *J. Appl. Phys.*, 1973, **44**, 5377–5382.

108 Y. Lee, T. Vogt, J. A. Hriljac, J. B. Parise and G. Artioli, *J. Am. Chem. Soc.*, 2002, **124**, 5466–5475.

109 Y. Lee, T. Vogt, J. A. Hriljac, J. B. Parise, J. C. Hanson and S. J. Kim, *Nature*, 2002, **420**, 485–489.

110 R. Arletti, E. Fois, L. Gigli, G. Vezzalini, S. Quartieri and G. Tabacchi, *Angew. Chem., Int. Ed.*, 2017, **56**, 2105–2109.

111 J. L. Jordá, F. Rey, G. Sastre, S. Valencia, M. Palomino, A. Corma, A. Segura, D. Errandonea, R. Lacomba, F. J. Manjón, Ó. Gomis, A. K. Kleppe, A. P. Jephcoat, M. Amboage and J. A. Rodrguez-Velamazán, *Angew. Chem., Int. Ed.*, 2013, **52**, 10458–10462.

112 A. U. Ortiz, A. Boutin, A. H. Fuchs and F.-X. Coudert, *J. Phys. Chem. Lett.*, 2013, **4**, 1861–1865.

113 P. Ballone, S. Quartieri, A. Sani and G. Vezzalini, *Am. Mineral.*, 2002, **87**, 1194–1206.

114 O. Ferro, S. Quartieri, G. Vezzalini, E. Fois, A. Gamba and G. Tabacchi, *Am. Mineral.*, 2002, **87**, 1415–1425.

115 C. Betti, E. Fois, E. Mazzucato, C. Medici, S. Quartieri, G. Tabacchi, G. Vezzalini and V. Dmitriev, *Microporous Mesoporous Mater.*, 2007, **103**, 190–209.

116 S. Ori, S. Quartieri, G. Vezzalini and V. Dmitriev, *Am. Mineral.*, 2008, **93**, 1393–1403.

117 M. Colligan, P. M. Forster, A. K. Cheetham, Y. Lee, T. Vogt and J. A. Hriljac, *J. Am. Chem. Soc.*, 2004, **126**, 12015–12022.

118 R. Arletti, G. Vezzalini, S. Quartieri, F. D. Renzo and V. Dmitriev, *Microporous Mesoporous Mater.*, 2014, **191**, 27–37.

119 S. C. McKellar and S. A. Moggach, *Acta Crystallogr., Sect. B: Struct. Sci., Cryst. Eng. Mater.*, 2015, **71**, 587–607.

120 J. Im, N. Yim, J. Kim, T. Vogt and Y. Lee, *J. Am. Chem. Soc.*, 2016, **138**, 11477–11480.

121 Y. A. Göğüs, *Energy Storage Systems. Mechanical Energy Storage*, UNESCO, 2009, vol. 1.

122 N. Giovambattista, P. G. Debenedetti and P. J. Rossky, *J. Phys. Chem. C*, 2007, **111**, 1323–1332.

123 J. K. Brennan, T. J. Bandosz, K. T. Thomson and K. E. Gubbins, *Colloids Surf., A*, 2001, **187-188**, 539–568.

124 T. Kimura, H. Kanoh, T. Kanda, T. Ohkubo, Y. Hattori, Y. Higaonna, R. Denoyel and K. Kaneko, *J. Phys. Chem. B*, 2004, **108**, 14043–14048.

125 T. Ohba and K. Kaneko, *J. Phys. Chem. C*, 2007, **111**, 6207–6214.

126 J.-C. Liu and P. A. Monson, *Langmuir*, 2005, **21**, 10219–10225.

127 R. Evans and U. M. B. Marconi, *J. Chem. Phys.*, 1987, **86**, 7138–7148.

128 R. Evans, *J. Phys.: Condens. Matter*, 1990, **2**, 8989–9007.

129 J. R. Henderson, in *Fundamentals of Inhomogeneous Fluids*, ed. D. Henderson, Marcel Dekker, 1992, ch. 2.

130 J. Israelashvili, in *Intermolecular and Surface Forces*, Academic Press, 2nd edn, 1992, ch. 13.

131 H. K. Christenson, *J. Chem. Phys.*, 1983, **78**, 6906–6913.

132 S. Granick, *Science*, 1991, **253**, 1374–1379.

133 I. Snook and W. van Megen, *J. Chem. Phys.*, 1979, **70**, 3099–3105.

134 M. Schoen, D. J. Diestler and J. H. Cushman, *J. Chem. Phys.*, 1987, **87**, 5464–5476.

135 P. Bordarier, B. Rousseau and A. H. Fuchs, *J. Chem. Phys.*, 1997, **106**, 7295–7302.

136 F. Porcheron, M. Schoen and A. H. Fuchs, *J. Chem. Phys.*, 2002, **116**, 5816–5824.

137 M. Heuberger, *Science*, 2001, **292**, 905–908.

138 E. W. Washburn, *Phys. Rev.*, 1921, **17**, 273–283.

This journal is © The Royal Society of Chemistry 2017

Chem. Soc. Rev., 2017, **46**, 7421–7437 | 7437